Harnessing Point-defect Induced Local Symmetry Breaking in the tetragonal-HfO2 System through Sterically Mismatched Ion Doping

Journal:	*Journal of Materials Chemistry C*
Manuscript ID	TC-ART-10-2023-003566.R2
Article Type:	Paper
Date Submitted by the Author:	25-Dec-2023
Complete List of Authors:	Bakhtiar, Syed Ul Hasnain; Huazhong University of Science and Technology, Ai, Po; Huazhong University of Science and Technology, School of Optical and electronic information Sattar, Harse; Huazhong University of Science and Technology, School of Integrated Circuits, Research Centre & Wuhan National Lab for Optoelectronics & Optical Valley Laboratory Ali, Sharafat; Heilongjiang University, Chemistry Al-Fatesh, Ahmed; King Saud University College of Engineering, Chemical Engineering Zhao, Junlei; Helsingin Yliopisto, Department of Physics and Helsinki Institute of Physics Wen, Dong; Huazhong University of Science and Technology, School of Integrated Circuits, Engineering Research Center for Functional Ceramics of the Ministry of Education & Wuhan National Laboratory for Optoelectronics Fu, Qiuyun; Huazhong University of Science and Technology(HUST), School of optical and electronic information; Huazhong University of Science and Technology(HUST) , State Key Laboratory of Material Processing and Die &Mould Technology

1   **Harnessing Point-defect Induced Local Symmetry Breaking in the**

2   **Tetragonal-HfO$_2$ System through Sterically Mismatched Ion Doping**

3   Syed Ul Hasnain Bakhtiar [a], Pu Ai [a], Harse Sattar [a], Sharafat Ali [b], Ahmed Sadeq Al-Fatesh [c],

4   Junlei Zhao [d]*, Wen Dong [a,e]*, Qiuyun Fu [a,e]*

5   [a] School of Integrated Circuits, Research Centre & Wuhan National Lab for Optoelectronics & Optical Valley
6   Laboratory Huazhong University of Science and Technology Wuhan 430074, China

7   [b] School of Physics, University of Electronic Science and Technology of China, Chengdu, 610054, China

8   [c] Chemical Engineering Department, College of Engineering, King Saud University, P.O. Box 800, Riyadh 11421,
9   Saudi Arabia

10   [d] Department of Electrical and Electronic Engineering, Southern University of Science and Technology, Shenzhen,
11   518055, China

12   [e] Shenzhen Huazhong University of Science and Technology Research Institute, Shenzhen 518000, P. R. China

13   Correspondence: zhaojl@sustech.edu.cn; dongw@hust.edu.cn; fuqy@mail.hust.edu.cn;

14   **Abstract**

15   Defect-engineering is a frequent approach to modify the material's properties. The selection of the

16   dopant is generally carried out by its similarity (size and valence state) to the host ions, which can

17   only slightly tune the properties of the host materials. In this work, opposing the traditional doping

18   approach, sterically mismatched 'difficult-to-dope' ions featuring different ionic sizes and valence

19   states were introduced as dopants, leading to local symmetry breaking. For this purpose, a non-

20   ferroelectric tetragonal-HfO$_2$ with a 4/mmm point group was doped with sterically mismatched

21   Y^{3+} / La^{3+} ions. The larger ionic radius of Y and La (106 pm and 110 pm, respectively) have been

22   expected to create a large point-defect-induced local symmetry breaking in the centrosymmetric

23   tetragonal environment. Density-functional-theory-based ab initio calculations were performed to

24   investigate the defect structure, where the local symmetry breaking and structural frustration

25   caused by Y^{3+} and La^{3+} dopant resulted in the total atomic displacement of 2.769 and 3.507 Å,

26   within the centrosymmetric environment. Importantly, this structural perturbation generates

27   noticeable defect-induced dipole moments of 7.07 Debye and 9.62 Debye for Y^{3+} and La^{3+},

28   respectively. The resultant dipole is attributed to the total ionic displacement of neighboring ions

1   caused by local symmetry breaking through sterically mismatched ions with different ionic sizes

2   (the larger the ionic size, the larger the ionic displacement and total dipole). In addition, La and Y

3   co-doped HfO_2 was also investigated, where the co-doping led to a total dipole in the range of 7.12

4   - 8.68 Debye. The defect-dipolar behavior may provide another insight to the understanding of the

5   polarization behavior in hafnium-based oxide as well as for manipulating material properties.

6   **Keywords:** Point-defects; Symmetry breaking; Ferroelectricity; HfO_2; Defect engineering

7   1. Introduction

8   Doping is a frequent approach used to alter or enhance the properties of host materials. [1-3] The

9   selection of the dopants is generally based on the similarity between the size and valence state of

10   the dopants and host ions; however, this approach can only slightly tune the characteristics of the

11   host materials. Notably, we have discovered the alternative approach of using "difficult to dope"

12   ions with sterically incompatible dopants, which further implement structural frustration, could be

13   a productive technique to drastically change the chemical environment and associated spatial

14   locality of the dopants, further modifying the properties of the host materials and even introducing

15   new functionalities. [2, 4, 5] This type of defect-driven geometry frustration frequently causes

16   spontaneous local symmetry breakdown in materials,[6] which then influences the material's

17   characteristics. As a result, the overall average structure does not change, but the features of the

18   system alter exceptionally. This defect-engineering is a bottleneck of advanced functional

19   materials, which can induce beyond average structural properties by induced defect-pair. The

20   discovery of high permittivity materials is strong evidence [7-9] where the host material is

21   synergistically doped with ions, including a "difficult-to-dope" ion, to produce massive defect

22   clusters in a steady state that yield electron-pinned defect dipoles. [10] For example, Ren et al. [11]

23   reported that oxygen vacancies (*Vo*) induced polarization changes, enhancing piezoelectric

24   properties in *c*-$BaTiO_3$. Therefore, understanding the point defects is crucial for designing and

25   optimizing new functional materials.

26   In ferroelectric materials, the polarization performance can be tuned by the point-defect-induced

27   dipole. In bulks, the point defects are suggested to induce larger strain [11], inducing a waist

28   polarization loop. Klyukin *et al* [12] investigated the effect of various intrinsic defects and defect

29   clusters in $SrTiO_3$, where the Sr and Ti antisite defects induced ferroelectric polarization to the

1   materials. Grünebohm *et al* [13] studied the ferroelectricity in $BaTiO_3$, where the parallel defect

2   dipoles resulted in an internal electrical field, leading to an enhanced polarization, accompanied

3   by a declining ferroelectric transition. Shimada *et al* [14] also investigated the effect of V_O on the

4   multi-ferroic behavior and electronic properties of $BiFeO_3$. Neutral V_O, as a deep donor, reduced

5   the magnetic moments at neighboring Fe^{3+} ions, and the charged V_O provides additional

6   ferroelectric polarizations.

7   The current research state of material and device needs further advancements. For example, huge

8   ferroelectricity was discovered in HfO_2 and ZrO_2-based materials. HfO_2-based ferroelectrics are

9   compatible with modern silicon-based information technologies.[15] This compatibility is crucial for

10 the integration of ferroelectric materials into non-volatile memory and advanced energy devices.[16]

11 Ferroelectricity in the HfO_2 system can be observed in its orthorhombic phase.[17] Moreover, to

12 investigate the impact of defect engineering and importing ferroelectricty through point-defect

13 induced local symmetry breaking in the system, a non-ferroelectric phase of the HfO_2 should be

14 selected. Literature is available where emergent ferroelectricity is theoretically found in non-

15 ferroelectric bulk-TiO_2,[18] and experimentally from $SrTiO_3$ and low free-standing $BaTiO_3$ ultrathin

16 film.[11] This defect-engineering is a bottleneck of advanced functional materials, which can induce

17 beyond average structural properties by induced defect-pair. In addition, the performance of HfO_2-

18 based ferroelectric devices during their life cycle is critically dependent on the presence of point

19 defects.[19] Therefore, it is requisite to use defect engineering to understand the structure and

20 polarization state of the point-defect-induced local symmetry breaking in different systems.

21 In this paper, to investigate the impact of defect engineering and importing ferroelectricity through

22 point-defect induced local symmetry breaking in the system, we have selected a non-ferroelectric

23 *tetragonal*-HfO_2 (*t*-HfO_2) as an example and a sterically mismatched "difficult-to-dope" ions of

24 Y^{3+} / La^{3+} having different ionic sizes and valence states were successfully doped in the HfO_2

25 lattice with different dimensions. The Y^{3+} / La^{3+} ion is bigger in size than the Hf^{4+} ion, with the

26 ionic radii being 106/ 110 pm compared to 85 pm, respectively. The large ionic radius of Y and

27 La have been expected to create a large point-defect-induced local symmetry breaking in the

28 centrosymmetric tetragonal environment. Defect-dipolar states of bulk Y/La-doped HfO_2 were

29 successfully calculated. We have achieved an obvious defect-dipolar moment of 7.07 and 9.62

30 Debye, respectively. For bulk non-ferroelectric *t*-HfO_2, the total free energy is mainly contributed

1   to the Landau bulk free energy and elastic free energy, where the former is far larger than the latter

2   one. Therefore, the contribution of elastic free energy due to point-defect-induced local symmetry

3   breaking is more prominent.

4   **2. DFT calculation method**

5   Density functional perturbation theory (DFPT) calculations were performed under periodic

6   boundary conditions using the projector-augmented wave (PAW) approach [20, 21] implemented in

7   the Vienna Ab initio simulation package (VASP) software [22, 23] using the Perdew–Burke–

8   Ernzerhof (PBE) functional [24] to study the point defect-induced local symmetry breaking in Y/La-

9   doped t-HfO$_2$ at different dimensions. The Perdew–Burke–Ernzerhof (PBE) [24-26 24-26 24-26 16-18 16-18]

10   functional under the generalized gradient approximation (GGA) is applied to deal with the

11   exchange and correlation interactions.

12   A t-HfO$_2$ with a 4/mmm point group and a cell length of a=b= 4.859 Å, c=3.224 Å was used

13   (Materials Project [27] ID: mp-776532, **Fig. S1(a-c)**). The Hf (4f, 5d, 6s), Y (4d, 5s), La (5s, 5p, 5d,

14   6s) and O (2s, 2p) electron orbitals are treated as valence states with the following atomic valence

15   configurations: Hf ($4f^{14}5d^26s^2$), Y($4d^15s^2$), La($5s^25p^65d^16s^2$) and O($2s^22p^6$). The cutoff energy of

16   plane wave is set to be 600 eV which is large enough for energy convergency. To figure out the

17   defect states with the lowest energy configuration, 2×2×2 supercells t-HfO$_2$ with a 4/mmm point

18   group were constructed. The 3×3×5 Monkhorst-Pack[28] k-points mesh is applied for the first

19   Brillouin zone of the 47-atom supercells for doped HfO$_2$. A non-spin-polarized calculations were

20   performed with a smearing value of 0.03 eV with a Gaussian smearing method and the force

21   tolerance for the structure optimization and total energy were respectively converged to 10^{-2}

22   eV • Å^{-1} and 10^{-6} eV.”

23   A 2×2×2 supercell was constructed for pure t-HfO$_2$ (**Fig. S1(d-f)**), where the defects (2Y or 2La)

24   were then substituted to replace two nearby or far Hf atoms with the Y^{3+} / La^{3+} doping level of

25   12.5%. Generally, replacing Hf^{4+} ions with Y^{3+} / La^{3+} can lead to significant over-bonding unless

26   an oxygen vacancy is created to counter the net charge of the super-structure. Therefore, an oxygen

27   vacancy was also created at a nearby or far away position to counter-balance the net charge of the

28   structure. Ionic relaxation was performed to allow the Hf and O ions to displace around the point

1   defect. The total energy of the system depends strongly on the locations of the dopants and oxygen

2   vacancy, where the one with oxygen vacancy in the vicinity between two dopants is the most stable.

3   Ionic displacements of the ions were calculated relative to the ionic position in the pure HfO_2. The

4   size and direction of the displacements showed the maximum displacement in the vicinity of the

5   oxygen position. To estimate the resulting polarization caused by the ionic displacements, density-

6   functional perturbation theory (DFPT) was used to calculate the Born effective charges (Z^n_{ij}). The

7   relationship between polarization and ionic displacements is shown below:

8
$$Z^n_{ij} = \frac{\Omega \partial P^n_i}{e \, \partial u^n_j} \tag{1}$$

9   where n is the numeric label unique to each Hf, Y/La, and O in the simulation, Ω is the unit cell

10 volume, e is the fundamental charge on an electron, P^n_i is the polarization component in the

11 Cartesian direction i, and u^n_j is the displacement of the ion in the Cartesian direction j. To estimate

12 the net change in polarization caused by the Y/La defect, the Born charge tensors for each ion were

13 multiplied by the displacement vector determined in the ionic relaxation and summed over all n

14 atoms in the simulation to give the net polarization along the direction i:

15
$$Pi = \sum_n^{n=N} Z^n_{ij} \, \partial u^n_j - P(0) \tag{2}$$

16 The reference state P(0) was taken against the undistorted structure of pure HfO_2.

17
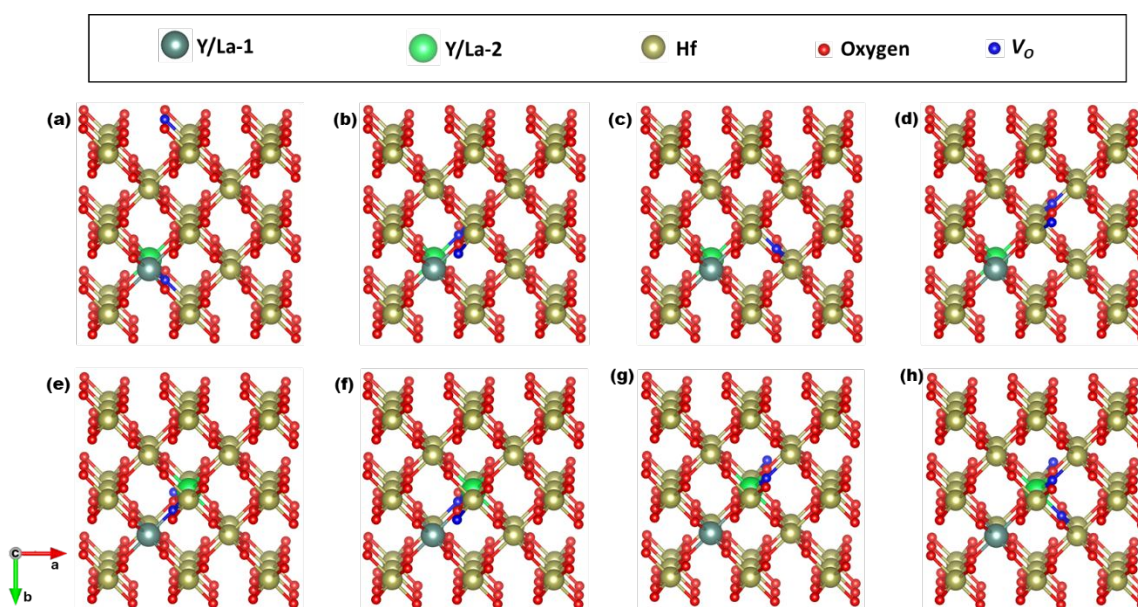
1. **Fig. 1** Possible defects structures of doped HfO_2, with two Y/La-ions at equatorial positions (a-d)

2. and polar-equatorial position (e-h). As two sterically mismatched Y^{3+} or La^{3+} ions were doped to

3. replace Hf^{4+} ions, the resulting over-bonding was satisfied by creating a V_O at nearby/far and

4. equatorial/polar position of Y-dopant. As two Y or La atoms were doped in the HfO_2 supercell to

5. induce defects, for clarification purposes, the Hf, Y1/La1, and Y2/La2 were distinguished by

6. golden, indigo, and light green color, respectively. In contrast, the O-ions and V_O were indicated

7. by red and blue color, respectively.

8. ## 3. Results

9. To investigate the structural optimization of the locally induced $Y-V_O$ defect in HfO_2, several

10. possible defect configurations based on the neighboring and far dopant-dopant ion position and

11. varying position of V_O were constructed to find out the total lowest energy configuration, as shown

12. in **Fig. 1(a-h)**. The Y1/La1 and Y2/La2 are distinguished by indigo and light green colors, while

13. the O-ion and O-vacancy (V_O) are distinguished by red and blue colors, respectively. The

14. comparison of the total minimum energy configurations between different configurations is

15. depicted in **Fig. 2(a-b)**.
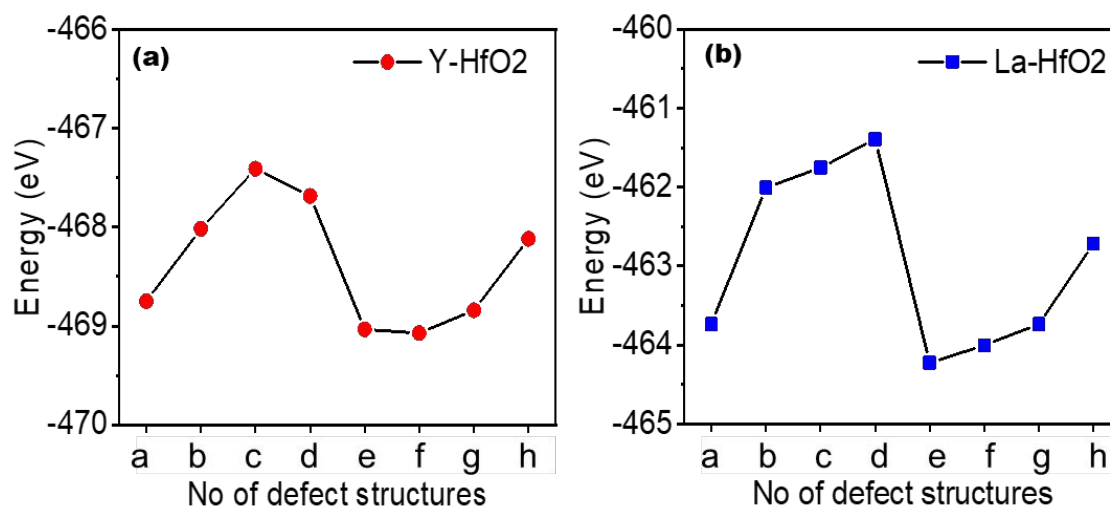
16.

17. **Fig. 2** Total minimum energy configurations of the defect system no. a-h correspondingly

18. presented in Figure 1(a-h). After relaxing all the defect structures through DFT-based first

1   principal calculation, the total lowest energy configuration for bulk La-doped HfO_2 and Y-doped

2   HfO_2 structure was found to be defect no (f) and (e), respectively.

3   For the bulk Y-doped HfO_2 case (**Fig. 2a**), the total lowest energy configuration was found to be

4   the one having V_O at the center of two doped Y-ions but neighboring Y2, as illustrated in **Fig. 1f**

5   and is considered as the local structure to be studied here. **Fig. 3a** presents the defect structure of

6   the Y-doped HfO_2, where significant ionic displacements were shown at the neighboring position

7   of V_O, as compared with pure-HfO_2. From **Fig. 3c**, the arrows reflect the displacement within the

8   crystal structure in all possible directions, where Ionic displacements relative to pure HfO_2 as a

9   function of radial distance from Y2-ion as a defect, lies within 8 Å away (while 10 Å from Y1-

10   ion, because the oxygen vacancy lies far away from Y1-ion rather than at neighboring position like

11   Y2-ion, **Fig. S2a**). Maximum displacement was observed in the vicinity of the point defect center

12    $(Y-V_O)$, with the maximum magnitude of the ionic displacements 0.299 Å and 0.229 Å for Hf and

13   O-ions, respectively (**Fig. 3c**).

14   To further elucidate the strategy, the defect structure of La-HfO_2 was also studied. The lowest

15   energy configuration for La-doped HfO_2 was found to have the V_O at the middle of two La-ions

16   but neighboring La1 (**Fig. 1e**). From **Fig. 3c**, it can be seen that the ionic displacements in the La-

17   doped HfO_2 defect structure relative to pure HfO_2 as a function of radial distance from the defect

18   La2 lies within the vicinity of 8 Å. The maximum displacement observed for Hf and O-ions is 0.35

19   Å and 0.33 Å, respectively (**Fig. 3d**). Moreover, the ionic displacements as a function of radial

20   distance from La1-ion as a defect also show the same pattern, corresponding to the same ionic size

21   (La-ion) and almost same distance from oxygen vacancy position (**Fig. S2b**).
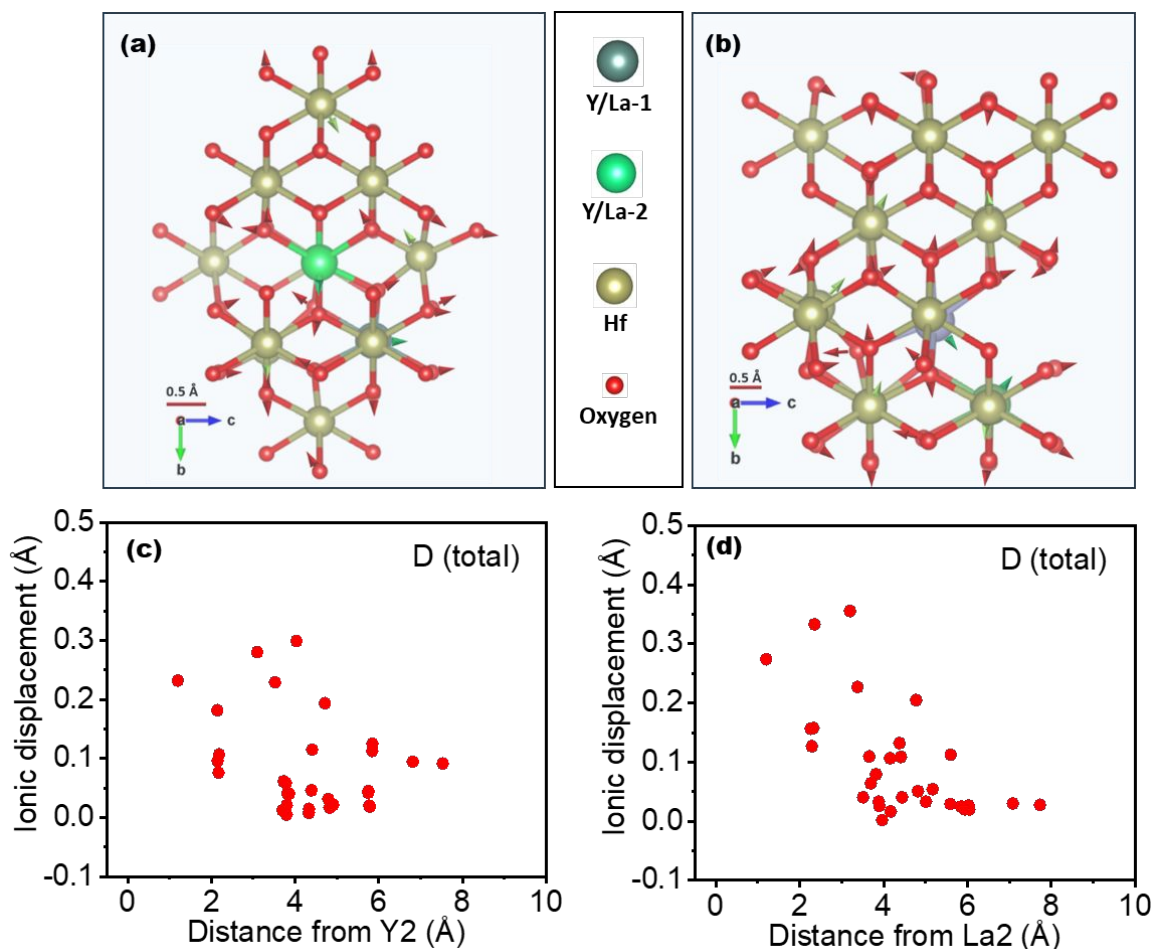
Fig. 3 DFT-based first principle calculations of local defects structure in bulk with 2×2×2 supercell structure, where Y-ions (a) and La-ions (b) were doped as a defect. In detail, the dopant-induced defect structures show significant ionic displacements as compared with pure HfO_2 where the direction of arrows reflects the ionic displacement within the crystal structure in all possible directions (a and e). Ionic displacement relative to pure HfO_2 as a function of radial distance from the selected Y2-ion (c) and La2-ion (d) as a defect lies within 8 Å from corresponding defects, where "D" represents total ionic displacement in all directions ($x+y+z$).

Furthermore, density-functional perturbation theory (DFPT) was used to calculate the Born effective charges of the ions, which will be further employed to calculate the net polarization caused by the defect-induced ionic displacements in the Y-doped HfO_2 structure. In detail, to estimate the net polarization change caused by the Y-V_O defects, the Born charge tensors for each ion were simply multiplied by the ionic displacement determined from the ionic relaxation step

1   (relative to the pure HfO_2 structure). The resultant ionic dipoles for individual ions are summed up

2   to get the net polarization magnitude. Except for the nearest neighbors to the $2Y_{Hf}$-$1V_O$ pairs, the

3   Born effective charges were found to be approximately constant for the Hf and O at 6 e (at z-axis)

4   and -3 e, respectively, as shown in **Fig. 4a**. Based on the ionic displacement and born effective

5   charge obtained by the Y-doped Hf_2O system, the calculated defect-induced polarization of 7.07

6   Debye was obtained in bulk Y-doped HfO_2 structure. Furthermore, the Born effective charges also

7   showed the same pattern as La-HfO_2, as shown in **Fig. 4b**. The resulting polarization magnitude

8   for bulk La-HfO_2 was 9.62 Debye as from **Fig. 4d**, higher but in the opposite direction as of Y-

9   HfO_2. The substantial enhancement in born effective charge for Hf is a typical feature for

10   ferroelectric systems or local symmetry breaking.[29-31] The DFT calculations, however, reveal a

11   more complex picture involving the collaboration of defects with the Hf displacements, leading to

12   minimized energy. In addition, Born-effective charges (a and c) and Dipole moment (b and d) vs

13   distance from defect for Y1 and La1 was also shown in **Fig. S3**, which also showing the same

14   pattern.

1
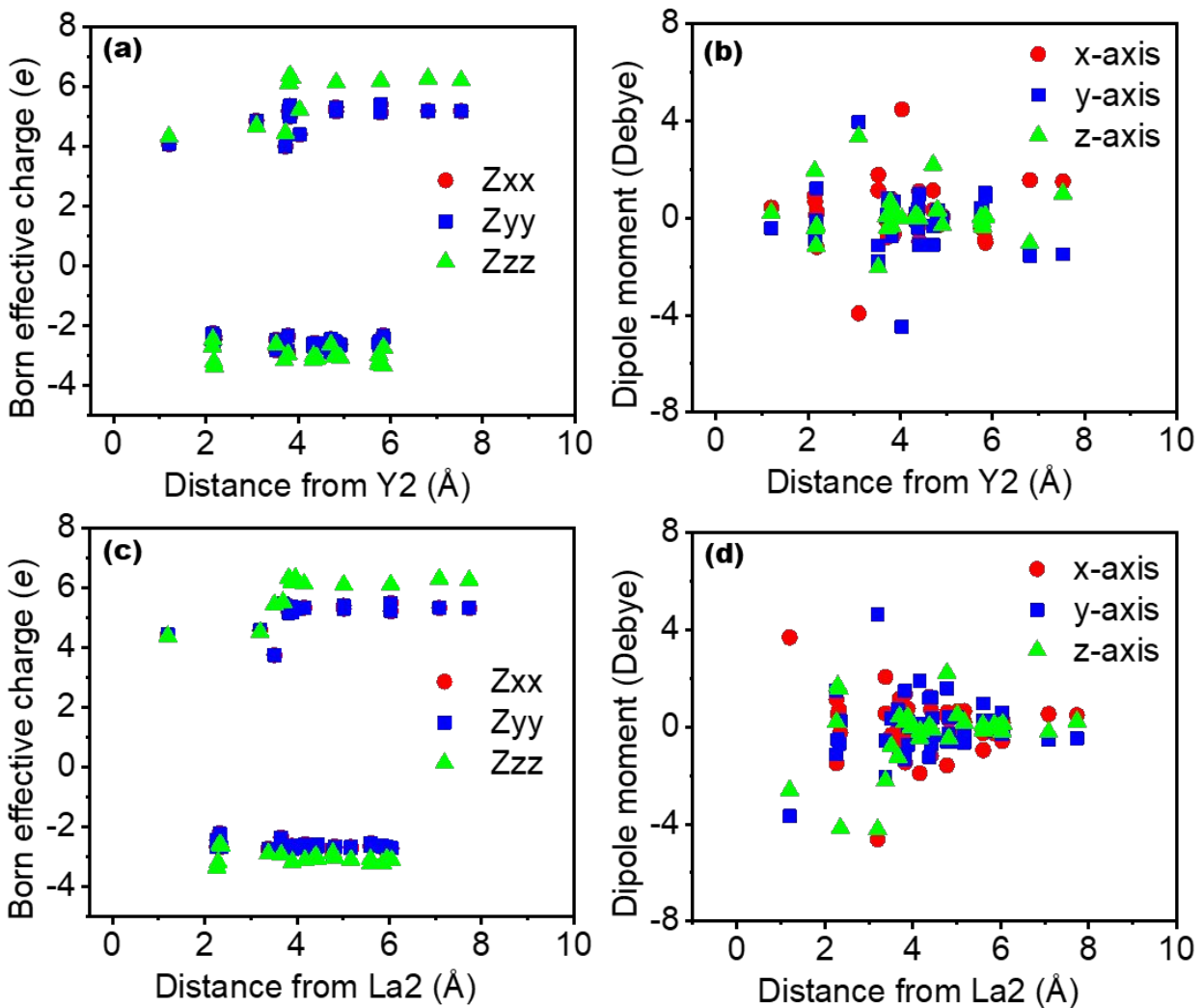
Fig. 4 Born-effective charges (a and c) and Dipole moment (b and d) vs distance from defect (only Y2 and La2 were taken into consideration) were also calculated based on Density Functional Perturbation Theory (DFPT) calculations.

To further extend the study, Y and La co-doping strategy was employed by taking the two lower energy configuration of Figure 1e and 1f, as employed for defect engineering of the sole Y/La-doped HfO$_2$ system as depicted in **Fig. 3** and **Fig. 4**. For each system, the position of single Y and La defects were exchanged while keeping the position of oxygen vacancy undisturbed, where the **Fig. 5(a-b)** represents the defect structure corresponding to **Fig. 3a** and **Fig.1e**. In contrast, **Fig. 5(c-d)** corresponds to the defects structure given in **Fig. 3b** and **Fig. 1f** (based on position of

1   oxygen vacancy), respectively. The Y and La were distinguished by indigo and light green colors,

2   while the O-ion and O-vacancy (VO) were distinguished by red and blue colors, respectively.

3
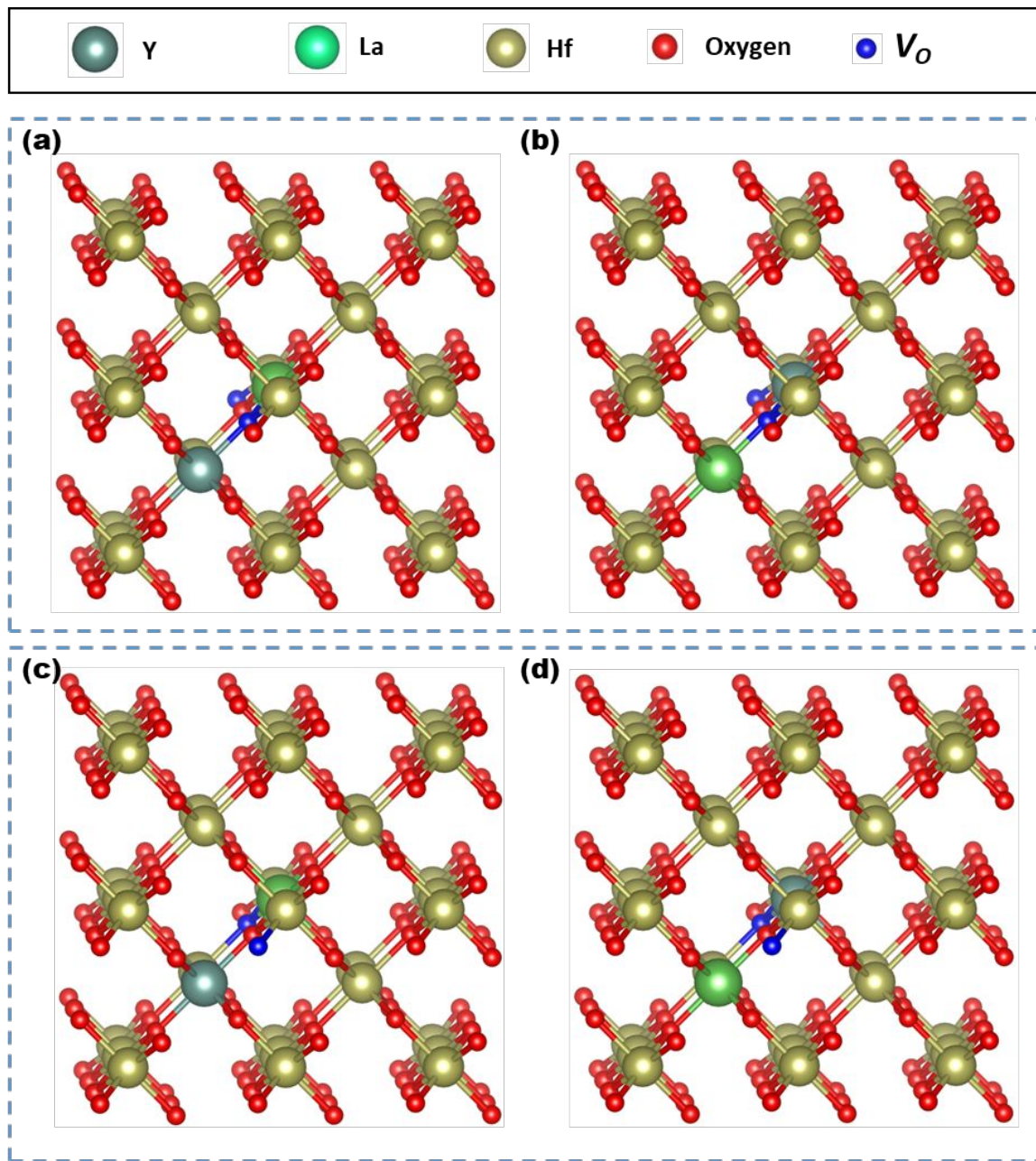
4   **Fig. 5** Defects structures of co-doped HfO_2, with one Y and one La-ions based on defects structure

5   presented in Figures 1e and 1f (differentiated by oxygen vacancy position). (a-b) corresponds to

6   the defect structure of Figure 1e, while (c-d) presents the defects corresponding to the defect

7   structure of Figure 1f with an interchanging position of Y and La dopant.

1   In a detailed study, **Fig. 6** presents the defect structure illustrated in **Fig. 5a,** having La-ion at the

2   center and the oxygen vacancy belonging to both La and Y-ion combinedly. The defect structure

3   after calculations presented a huge displacement of the ions in the vicinity of defects and oxygen

4   vacancy, as presented in **Fig. 6b,** while the magnitude of displacement with respect to distance

5   from defects Y and La were shown in **Fig. 6c** and **6d,** respectively. It can be seen that the ionic

6   displacement, as a function of radial distance from La and Y as a defect, lies within 8 Å away from

7   the defects La and Y because the oxygen vacancy lies in the mid position of both defects, where a

8   maximum magnitude if ionic displacement were calculated to be 0.32 Å. In addition, a higher

9   magnitude of displacement was observed within close vicinity of La as compared with Y-ion,

10   which may be attributed to the difference in the ionic size of the defects. Based on the ionic

11   displacement and born effective charge obtained, the ionic dipoles for individual ions are

12   calculated as presented in **Fig. 6 (e-f)** where a total magnitude of the defect-induced polarization

13   of 8.68 Debye was obtained.
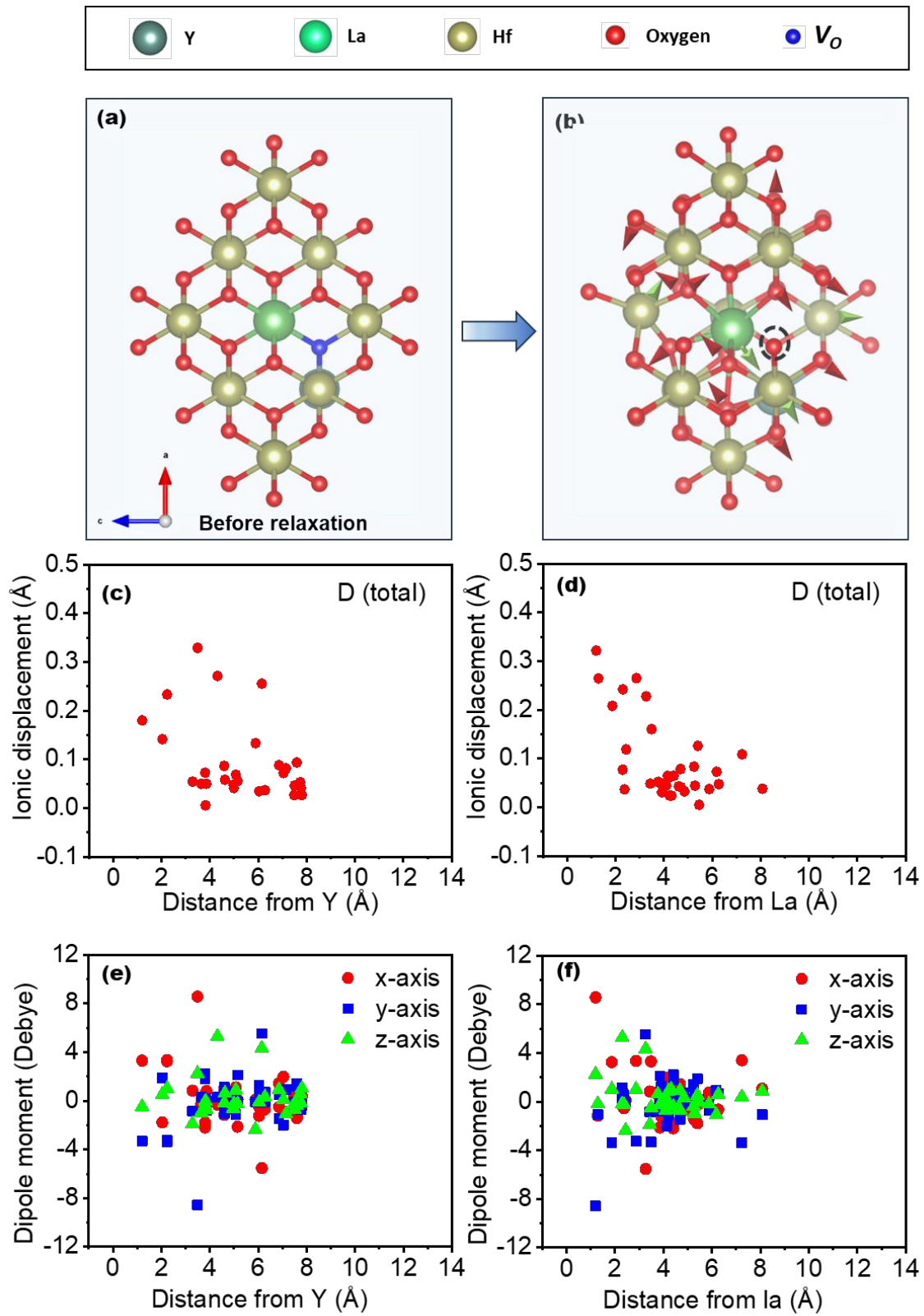
Fig. 6 DFT-based first principle calculations of local defects structure, where Y-ions and La-ions were co-doped as a defect in HfO_2, based on the defect structure presented in Figure 5a. (a) the structure before relaxation and (b) the dopant-induced defect structures showing significant ionic displacements were presented. Ionic displacement as a function of radial distance from the selected dopant (c) Y and (d) La as a defect lies within 8 Å from corresponding defects, respectively. (where "D" represents total ionic displacement in all directions ($x+y+z$)). The calculated Dipole moment vs distance from defect (e) Y and (f) La were also presented.

Fig. 7 presents the defect structure presented in **Fig. 5b,** having Y-ion at the center and the oxygen vacancy belonging to both La and Y-ion combinedly. In this system, almost the magnitude of displacement was observed as compared with the defect system presented in **Fig. 6**. It can be seen that the ionic displacement as a function of radial distance from La and Y as a defect, still lies within 8 Å away attributing to the same position for oxygen vacancy, with a maximum magnitude if the ionic displacement of 0.31 Å. In addition, although in this system, the position of defects La and Y are interchanged compared to the defect structure presented in **Fig. 6**, the higher magnitude of displacement occurs in the close vicinity of La rather than Y-ion. It means the displacement distance from the defects depends upon the ionic size of the defect ion. The individual ionic dipoles for each ion are calculated as presented in **Fig. 7 (e-f)** where a total magnitude of the defect-induced polarization of 8.26 Debye was observed.
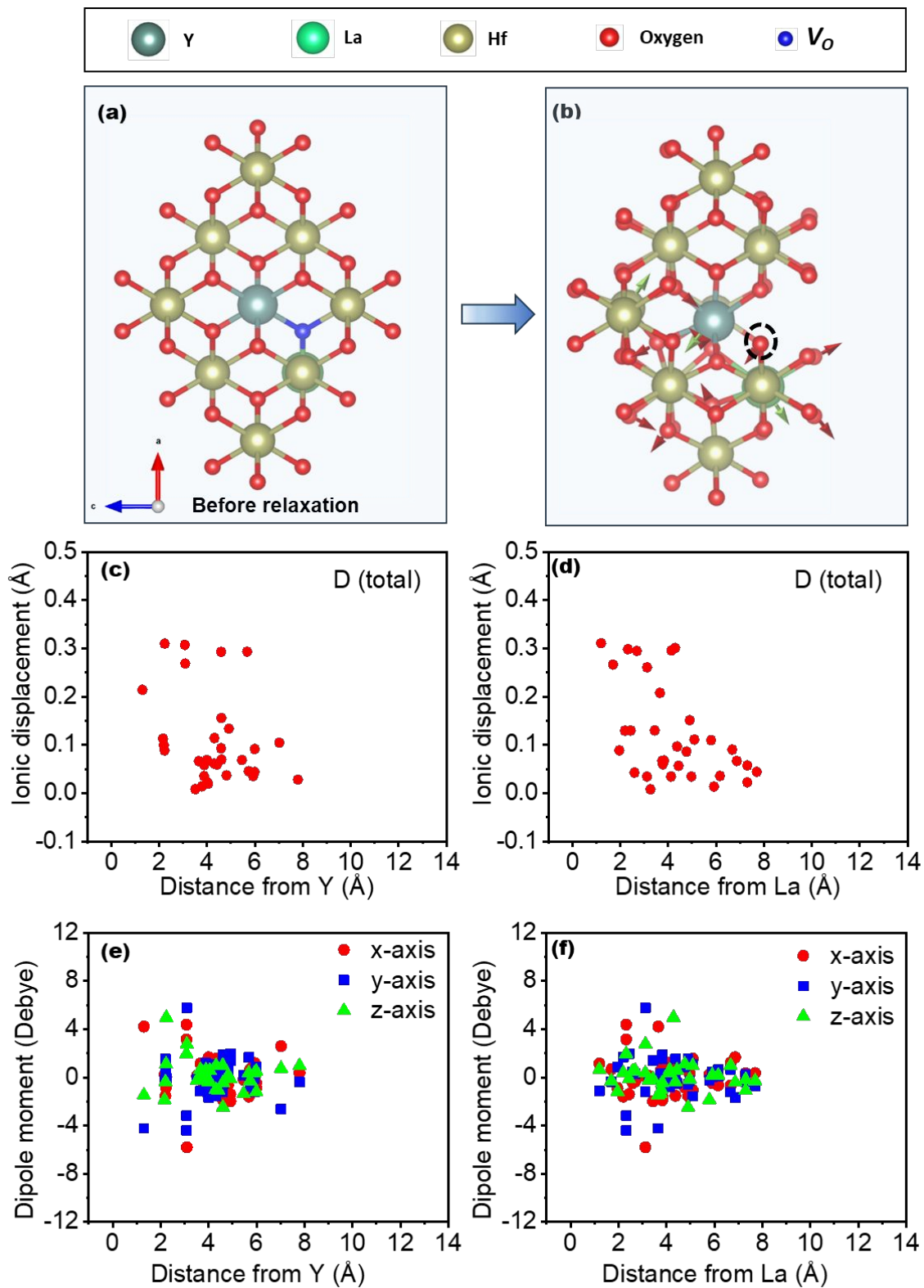
1   **Fig. 7** DFT-based first principle calculations of local defects structure, where Y-ions and La-ions

2   were co-doped as a defect in HfO2, based on the defect structure presented in Figure 5b. (a) the

3   structure before relaxation, and (b) the dopant-induced defect structures showing significant ionic

4   displacements were presented. Ionic displacement as a function of radial distance from the selected

5   dopant (c) Y and (d) La as a defect lies within 8 Å from corresponding defects, respectively. (where

6   "D" represents total ionic displacement in all directions (x+y+z)). The calculated Dipole moment

7   vs distance from defect (e) Y and (f) La were also presented.

8   Another study was also carried out (analogous to the defect structure presented in Fig. 6-7, based

9   on the position of oxygen vacancy), the defect structure shown in **Fig. 5(c-d)** having one defect

10   (Y/La) at the center and the oxygen vacancy belongs to the sole central defect only (**Fig. S4**

11   presents the La-ion at the center of the system, while the **Fig. S5** present the Y-ion at the center of

12   the system, where oxygen vacancy lies at the neighboring position of central defect only). In these

13   systems, it can be seen that the magnitude of maximum displacement is almost the same as the

14   above-mentioned system, with a value of 0.31 Å. From **Fig. S4(d),** we can see that ionic

15   displacement as a function of radial distance from La lies within 8 Å away, but the ionic

16   displacement as a radial distance from Y-defect lies with an expanded range of 10 Å as from **Fig.**

17   **S4(c)**. This can be attributed to the fact that for **Fig. S4(a-b)** we can see that the oxygen vacancy

18   lies neighboring to the La-ion but far away from Y-ion. Furthermore, the same pattern was

19   observed for the system presented in **Fig. S5** (interchanged Y and La-ion position while keeping

20   the position of oxygen vacancy the same), but with the ionic displacement within 8 Å from Y-ion

21   and 10 Å from La-ion, respectively. The individual ionic dipole calculated for both systems were

22   depicted in **Fig. S4(e-f)** and **Fig. S5(e-f),** respectively, where the sum of total dipole calculated for

23   these two systems were 7.12 and 7.5 Debye, respectively.

24   **4. Discussion**

25   The given DFT calculations explore the intriguing dynamics within doped HfO_2 structures,

26   particularly regarding the emergence of a defect dipole induced by the presence of specific dopants,

27   like Yttrium (Y) and Lanthanum (La). Herein, by taking *tetragonal*-HfO_2 (*t*-HfO_2) as an example

28   and the doping of the sterically mismatched "difficult-to-dope" ions of Y^{3+} / La^{3+} having different

29   ionic sizes and valence states were successfully carried out. To counterfeit the effect of over-

1   bonding during replacing Hf^{4+} ions with sterically mismatched Y^{3+} / La^{3+}, an oxygen vacancy was

2   also created at different positions to counter-balance the net charge of the super-structure.

3   The large ionic radius of Y^{3+} and $La^{3+,}$ accompanied by oxygen vacancy, have created a large

4   point-defect-induced local symmetry breaking in the centrosymmetric tetragonal environment,

5   resulting in a defect dipole. This defect dipole initiates a cascading effect, compelling neighboring

6   Hf and O ions to displace significantly, resulting in a "super-dipole". In a crystal lattice, when ions

7   are displaced from their equilibrium positions, they can create electric dipoles. The polarization of

8   a material is the vector sum of all these individual ionic dipoles. The key insight is the

9   manifestation of a net polarization in these systems, a quality absent in the conventional non-

10 ferroelectric tetragonal HfO_2, driven mainly by the nucleation of defect dipoles and subsequent

11 ion displacements. In this case, the polarization magnitude is being calculated for defect structures

12 in Y-doped and La-doped HfO_2. There is no dipole moment for conventional non-ferroelectric

13 bulk tetragonal HfO_2 (t-HfO_2).

14 The DFT calculations suggest that for Y-doped HfO_2 structure, a defect dipole is nucleated by the

15 presence of $2Y_{Hf}$-$1V_O$, which drives surrounding Hf-ions and O-ions to move off-center with large

16 displacement. It is important to note that the polarization is induced by displacements within 8 Å

17 range from Y2 ionic position and within 10 Å from Y1 ion, with the maximum magnitude of the

18 ionic displacements 0.299 Å and 0.229 Å for Hf and O-ions, respectively, where a maximum

19 displacement was observed in the vicinity of the point defect center ($Y-V_O$). In addition, the same

20 pattern of defect structure was observed for La-doped HfO_2, where the ionic displacements relative

21 to pure HfO_2 as a function of radial distance from the selected La2-ions and La1 ion as a defect

22 also lie within 8 Å and 10 Å, respectively, but with a maximum displacement of 0.35 Å and 0.33

23 Å for Hf and O-ions, respectively.

24 The comparison between Y-doped and La-doped HfO_2 unveils an interesting pattern: the greater

25 ionic size of La ions (110 pm), in contrast to Y ions (106 pm), leads to a more pronounced

26 displacement of neighboring ions in the vicinity of the defect center. This discrepancy in ionic size

27 contributes to a more substantial stress or distortion in the structure of La-doped HfO_2, thus

28 yielding larger maximum ionic displacements. This, in turn, accounts for the observed higher

29 magnitude of resultant polarization in La-doped HfO_2 compared to Y-doped HfO_2, emphasizing

the role of ion size in shaping the material's properties. The larger displacement observed with La doping suggests that La-doped HfO_2 may have different or enhanced properties than Y-doped HfO_2.

The Born effective charges for La-doped HfO_2 show the same pattern as Y-doped HfO_2. The Born effective charge measures how an ion's charge changes when displaced from its equilibrium position. The fact that the pattern is the same for both types of doping suggests that the doping process has a similar effect on the charge distribution in the material, regardless of whether Y or La ions are used.

To estimate the net polarization change caused by the Y/La-V_O defects, the Born charge tensors for each ion were multiplied by the ionic displacement determined from the ionic relaxation step (relative to the pure HfO_2 structure) and the resultant ionic dipoles for individual ions are summed up to get the net polarization magnitude. The resulting net polarization, estimated through the summation of individual ionic dipoles, exhibits a substantial difference between the Y-doped and La-doped structures. The defect structure containing 2YHf-1V_O in Y-doped HfO_2 presents a polarization magnitude of 7.07 Debye. In contrast, the bulk La-doped HfO_2 displays a higher polarization magnitude of 9.62 Debye, reflecting the influence of larger ion displacements and the resultant greater stress in the La-doped structure. This is because the larger ionic size of La (compared to Y) causes a more significant displacement of the surrounding ions, resulting in a larger total dipole moment and a larger polarization magnitude. This discrepancy in total dipole underscores the significance of dopant ions in dictating the polarization magnitude in these doped HfO_2 systems, emphasizing how subtle variations in dopant characteristics can significantly impact the material's properties.

To further extend the study, the Y and La co-doping strategy was employed by taking the two lower energy configurations of Figure 1e and 1f, as employed for defect engineering of the sole Y/La- doped HfO_2 system as depicted in **Fig. 3** and **Fig. 4**. For each system, the position of single Y and La defects were exchanged while keeping the position of oxygen vacancy undisturbed.

It was observed that for a system having oxygen vacancy is located at a neighboring position to both Y and la ions, the ionic displacement as a function of radial distance from La and Y as a defect lies within 8 Å away from the defects La and Y but for the system where the La-ion present

at the center at neighboring position of the oxygen vacancy and the Y-ion is located far from the oxygen vacancy, the ionic displacement as a function of radial distance from La lies within 8 Å away, but the ionic displacement as a radial distance from Y-defect lies with an expanded range of 10 Å (Fig. S4c). In addition, for the co-doped system, the higher magnitude of displacement was observed with a close vicinity of La as compared with Y-ion, which may be attributed to the difference in the ionic size of the defects. Based on the ionic displacement and born effective charge obtained, the ionic dipoles for individual ions are calculated, where a total magnitude of the defect-induced polarization observed for the co-doped system lies in the range of 7.12 to 8.68 Debye, which is greater than sole Y-doped system and lower than sole La-based HfO_2 system.

Overall, these findings underscore the intricate relationship between dopant characteristics, defect formation, ionic displacements, and resultant polarization in doped HfO_2 structures. The comparison between Y and La dopants and their relationship during co-doping sheds light on their distinct influences on the material's behavior. It highlights the importance of ion size in governing emergent properties, offering valuable insights for tailored material design and functional applications in ferroelectric systems.

In conclusion, this study also provides theoretical evidence that defect-driven symmetry breaking can achieve a larger magnitude of polarization in defect doped-HfO_2. As higher defect-induced polarization was obtained in both bulk Y-doped, La-doped, and co-doped-HfO_2 structures, on this basis, a 2D thin layer of Y-HfO_2 is under investigation and will be published in our next article. Thus, with further advancement in understanding the defects dipole mechanism, it is highly possible to produce materials with higher polarizations, e.g., by using other forms of sterically mismatched dopant and their doping concentration. This work advances our fundamental understanding of materials by harnessing the unique structural frustrations and enhanced defect-related phenomena induced by sterically mismatched dopants. It also promises transformative implications for developing advanced functional materials with tailored properties and improved performance. The defect-dipolar behaviors may provide another insight to the understanding of the polarization behavior in hafnium-based oxide as well as for manipulating material properties.

5. Summary

In summary, traditional doping is often carried out to tune the properties of the host materials, where the substitutional ions usually have the same size and electronegativity. Here, we introduced a "difficult-to-dope" ion by local symmetry breaking through defect engineering to import polarization. To achieve our goal, sterically mismatched Y^{3+} / La^{3+} ions (with different ionic sizes) were doped in a non-ferroelectric t-HfO_2 with 4/mmm point group, which led to structural frustration in the local environment. To comply with the different valence states of dopant and host ions, an oxygen vacancy was created in the defect structure to satisfy the total charge of the defect structure. Several possible defect structures were constructed to determine the lowest energy configuration of bulk Y/La-doped HfO_2. The doped ions drive surrounding Hf-ions and O-ions to move off-center, where a maximum displacement was observed in the vicinity of the point defect center (Y/La–V_O), with the maximum magnitude of the ionic displacements for Hf and O-ions observed to be 0.299 Å and 0.229 Å, for Y-HfO_2 and 0.35 Å and 0.33 Å for La-HfO_2, respectively. In addition, an obvious defect-dipolar moment of 7.07 and 9.62 Debye was found for bulk Y-HfO_2 and La-HfO_2, respectively. The resulting total dipole is attributed to the total ionic displacement caused by local symmetry breaking through sterically mismatched ions with different ionic sizes (the larger the ionic size, the larger the ionic displacement and total dipole). In addition, for La and Y co-doped HfO_2 system, the co-doping of HfO_2 with one Y and on La ions (having different ionic sizes) with different oxygen vacancy positions led to the comparatively smaller magnitude of total displacement (as compared with sole La doping) and lead to total dipole in the range of 7.12 - 8.68 Debye. This study provides theoretical evidence that defect-driven symmetry breaking can achieve a larger magnitude of polarization in defect doped-HfO_2. Thus, with further advancement in understanding the defects dipole mechanism, it is highly possible to produce materials with higher polarizations, e.g., by using other forms of sterically mismatched dopant and their doping concentration.

1   the   Researchers   Supporting   Project   number   (RSP2024R368)   of   King   Saud

2   University, Saudi Arabia.

3   **Authors Contribution**

4   WD and QF initiated the project. SHB ran the calculation with the assistance from PA, SA and

5   HS. WD and QF analyzed the data with the assistance of ZJ. SHB and WD wrote the manuscript.

6   **Data availability**

7   The data supporting this study's findings are available from the corresponding author, Professor

8   Wen Dong, upon reasonable request.

9   **Conflicts of interest**

10   The authors declare that they have no known competing financial interests or personal

11   relationships that could have appeared to influence the work reported in this paper.

12   **References**

13   1.   I. Grinberg, D. V. West, M. Torres, G. Gou, D. M. Stein, L. Wu, G. Chen, E. M. Gallo, A. R. Akbashev and P. K.
14   Davies, Perovskite oxides for visible-light-absorbing ferroelectric and photovoltaic materials, *Nature*, 2013, **503**, 509-
15   512.
16   2.   W. Hu, Y. Liu, R. L. Withers, T. J. Frankcombe, L. Norén, A. Snashall, M. Kitchin, P. Smith, B. Gong and H. Chen,
17   Electron-pinned defect-dipoles for high-performance colossal permittivity materials, *Nature materials*, 2013, **12**, 821-
18   826.
19   3.   A. Walsh and A. Zunger, Instilling defect tolerance in new compounds, *Nature materials*, 2017, **16**, 964-967.
20   4.   Q. Sun, C. Zheng, L. Q. Huston, T. J. Frankcombe, H. Chen, C. Zhou, Z. Fu, R. L. Withers, L. Norén and J. E. Bradby,
21   Bimetallic ions codoped nanocrystals: doping mechanism, defect formation, and associated structural transition, *The*
22   *Journal of Physical Chemistry Letters*, 2017, **8**, 3249-3255.
23   5.   Q. Sun, D. Cortie, S. Zhang, T. J. Frankcombe, G. She, J. Gao, L. R. Sheppard, W. Hu, H. Chen and S. Zhuo, The
24   formation of defect‐pairs for highly efficient visible‐light catalysts, *Advanced Materials*, 2017, **29**, 1605123.
25   6.   K. Pyka, J. Keller, H. Partner, R. Nigmatullin, T. Burgermeister, D. Meier, K. Kuhlmann, A. Retzker, M. B. Plenio and
26   W. Zurek, Topological defect formation and spontaneous symmetry breaking in ion Coulomb crystals, *Nature*
27   *communications*, 2013, **4**, 1-6.
28   7.   A. Tkach, O. Okhay, A. Almeida and P. M. Vilarinho, Giant dielectric permittivity and high tunability in Y-doped
29   SrTiO3 ceramics tailored by sintering atmosphere, *Acta Materialia*, 2017, **130**, 249-260.
30   8.   D. Huang, Z. Liu, Y. Li and Y. Liu, Colossal permittivity and dielectric relaxation of (Li, In) Co-doped ZnO ceramics,
31   *Journal of Alloys and Compounds*, 2017, **698**, 200-206.
32   9.   Y. Song, X. Wang, X. Zhang, X. Qi, Z. Liu, L. Zhang, Y. Zhang, Y. Wang, Y. Sui and B. Song, Colossal dielectric
33   permittivity in (Al + Nb) co-doped rutile SnO2 ceramics with low loss at room temperature, *Applied Physics Letters*,
34   2016, **109**, 142903.
35   10.   W. Hu, Y. Liu, R. L. Withers, T. J. Frankcombe, L. Norén, A. Snashall, M. Kitchin, P. Smith, B. Gong, H. Chen, J.
36   Schiemer, F. Brink and J. Wong-Leung, Electron-pinned defect-dipoles for high-performance colossal permittivity
37   materials, *Nature Materials*, 2013, **12**, 821-826.
38   11.   X. Ren, Large electric-field-induced strain in ferroelectric crystals by point-defect-mediated reversible domain
39   switching, *Nature materials*, 2004, **3**, 91-94.
40   12.   K. Klyukin and V. Alexandrov, Effect of intrinsic point defects on ferroelectric polarization behavior of SrTiO 3,
41   *Physical Review B*, 2017, **95**, 035301.

13.   A. Grünebohm and T. Nishimatsu, Influence of defects on ferroelectric and electrocaloric properties of BaTiO 3, *Physical Review B*, 2016, **93**, 134101.

14.   T. Shimada, T. Matsui, T. Xu, K. Arisue, Y. Zhang, J. Wang and T. Kitamura, Multiferroic nature of intrinsic point defects in BiFeO 3: A hybrid Hartree-Fock density functional study, *Physical Review B*, 2016, **93**, 174107.

15.   M. Dogan, N. Gong, T.-P. Ma and S. Ismail-Beigi, Causes of ferroelectricity in HfO2-based thin films: an ab initio perspective, *Physical Chemistry Chemical Physics*, 2019, **21**, 12150-12162.

16.   H. A. Hsain, Y. Lee, M. Materano, T. Mittmann, A. Payne, T. Mikolajick, U. Schroeder, G. N. Parsons and J. L. Jones, Many routes to ferroelectric HfO2: A review of current deposition methods, *Journal of Vacuum Science & Technology A*, 2021, **40**.

17.   S. K. Lee and C. W. Bark, Crystallographic structure and ferroelectricity of epitaxial hafnium oxide thin films, *Journal of the Korean Ceramic Society*, 2022, **59**, 25-43.

18.   W. Dong, D. Cortie, T. Lu, Q. Sun, N. Narayanan, W. Hu, L. Jacob, Q. Li, D. Yu, H. Chen, A. Chen, X. Wei, G. Wang, M. G. Humphrey, T. J. Frankcombe and Y. Liu, Collective nonlinear electric polarization via defect-driven local symmetry breaking, *Materials Horizons*, 2019, **6**, 1717-1725.

19.   A. Chouprik, D. Negrov, E. Y. Tsymbal and A. Zenkevich, Defects in ferroelectric HfO2, *Nanoscale*, 2021, **13**, 11635-11678.

20.   P. E. Blöchl, Projector augmented-wave method, *Physical Review B*, 1994, **50**, 17953-17979.

21.   G. Kresse and D. Joubert, From ultrasoft pseudopotentials to the projector augmented-wave method, *Phys. Rev. B*, 1998, **59**.

22.   G. Kresse and J. Furthmüller, Efficiency of ab-initio total energy calculations for metals and semiconductors using a plane-wave basis set, *Computational Materials Science*, 1996, **6**, 15-50.

23.   G. Kresse and J. Furthmiiller, Efficiency of ab-initio total energy calculations for metals and semiconductors using a plane-wave basis set, *Comp. Mater. Sci.* , 1996, **6**, 15-50.

24.   J. P. Perdew, K. Burke and M. Ernzerhof, Generalized Gradient Approximation Made Simple, *Physical Review Letters*, 1996, **77**, 3865-3868.

25.   D. Vanderbilt, Soft self-consistent pseudopotentials in a generalized eigenvalue formalism, *Phys. Rev. B. Condens. Matter.* , 1990, **41**, 7892-7895.

26.   J. P. Perdew, K. Burke and M. Ernzerhof, Generalized Gradient Approximation Made Simple, *Phys. Rev. Lett*, 1996, **77**, 3865.

27.   A. Jain, S. P. Ong, G. Hautier, W. Chen, W. D. Richards, S. Dacek, S. Cholia, D. Gunter, D. Skinner, G. Ceder and K. A. Persson, Commentary: The Materials Project: A materials genome approach to accelerating materials innovation, *APL Materials*, 2013, **1**.

28.   D. J. Chadi, Special points for Brillouin-zone integrations, *Phys. Rev. B*, 1977, **16**, 1748-1749.

29.   S. E. Rowley, L. J. Spalek, R. P. Smith, M. P. M. Dean, M. Itoh, J. F. Scott, G. G. Lonzarich and S. S. Saxena, Ferroelectric quantum criticality, *Nat. Phys.*, 2014, **10**, 367-372.

30.   M. E. Lines, Glass, A. M., Principles and applications of ferroelectrics and related materials, *Clarendon Press, Oxford, 1977*, 1977.

31.   W. Dong, D. Cortie, T. Lu, Q. Sun, N. Narayanan, W. Hu, L. Jacob, Q. Li, D. Yu, H. Chen, A. Chen, X. Wei, G. Wang, M. G. Humphrey, T. J. Frankcombe and Y. Liu, Collective nonlinear electric polarization via defect-driven local symmetry breaking, *Mater. Horiz.*, 2019, **6**, 1717-1725.